Synthesis and Spectroscopic Mixed Ligands Complexes of flavonoid and their Biological Study in Antitumor Activity for Treatment Breast Cancer Cell Line (MCF-7), Inhibitory Effect on Xanthine Oxidase and Antimicrobial

Ezalden J. Alobaidi
Department of Chemistry, College of Science, University of Anbar, Ramadi, Iraq, ez.jm.alobaidy@gmail.com

Omar H. Al-obaidi
Department of Chemistry, College of Science, University of Anbar, Ramadi, Iraq

Abstract

The present study, the chalcone was prepared by Claisen-Schmidt condensation. Utilizing the spectrometers shown (FT-IR, UV-Vis, 1H-NMR, 13C-NMR, and mass spectra), the synthesized compound was then evaluated. A new complexes was synthesized used the chalcone (HL1) as primary ligand and amino acid serine (HL4) as secondary ligand with [Co (II), Ni (II), Cu (II), Zn (II), and Cd (II)] ions. Additionally, using the spectroscopic techniques, all of the generated complexes have been identified (FT-IR, UV-Vis, 1H-NMR, 13C-NMR, magnetic susceptibility and conductivity studies). In the study findings indicated that all complexes had octahedral geometry and were nonconductive as measured by magnetic moments and molar conductance. The chalcone (HL1) and its copper complex were evaluated on the breast cancer cell line MCF-7 at dosages of (12.5, 25, 50, 100, 200) µg/ml, and the rate of cell growth inhibition was tracked for 48 hours of treatment. Comparing the effects of the copper complex and ligand on the MCF-7 breast cancer cell line before and after treatment, it was shown that the copper complex achieved good inhibition outcomes. The inhibition rate of ligand (HL1) and Cupper complex between (1.66 – 71.00), IC50 = 47.98 µg/ml and IC50 = 28.09 µg/ml, respectively. The ability of chalcone (HL1) and its complexes with cobalt and copper to inhibit xanthine oxidase was studied. The inhibition was studied by monitoring the xanthine absorbance at the wavelength of 290 nm. The results showed good inhibition ratios, and that the copper complex gave the highest inhibition rates, with IC50 values of [Cu(L1)(L4)(H2O)2] = 2.36 *10-5 molar, [Cu(L1)(L4)(H2O)2] = 2.73 *10-5 molar, and HL1 = 4.79*10-5M molar. Three different types of bacteria were used to study the biological activity of the synthesized ligands and their complexes with concentration (1×10-2, 1×10-3, 1×10-4) molar utilizing the inhibition approach (Staphylococcus aureusa, Escherichia coli and Burkholderia cepacia). To measure its potential antibacterial effect, this was done. The experiments generally indicated that the ligands and their complexes have modest or moderate action against the different kinds of bacteria and as follow:

Staphylococcus aureus > Escherichia coli > Burkholderia cepacia

Keywords: *chalcone, amino acid, serine, mix ligand, Metal complexes, anticancer cell line, xanthine oxidase inhibiting, antibacterial.*

INTRODUCTION

Chalcones are secondary metabolites of a plant that are either edible or therapeutic, and they belong to the flavonoid family. Chalcone is made up of two aryl moieties linked by an, α,β-unsaturated carbonyl group. They are 1,3-diphenyl-2-propen-1-ones (1). The structure of these compounds has a C═O-CH═CH- keto ethylenic moiety. They feature a delocalized -electron-containing arrangement in their

aromatic rings (2). Chalcone is mostly composed of polyphenolic substances with hues ranging from yellow to orange, and they play a key role in the coloration of various plant's corollas. Chalcone, which are found naturally in a variety of foods, including fruits, spices, teas, and soy products, have generated a great deal of attention due to their unique and perhaps beneficial properties. Additionally, pheromones, plant allelochemicals, and insect hormones are examples of these compounds in natural goods (3,4). The 20 amino acids are the fundamental building blocks of proteins and each one consists of an amino group (-NH2), a carboxyl group (-COOH), a hydrogen atom, and a (variable) distinctive (R) group. In an amino acid, each substituent is linked to a central α carbon atom through covalent bonds. The carboxyl (acidic) group and α carbon are joined (5). The biological uses of complex of metal ions and amino acids are important. Many researchers investigated the synthesis of intricate mixtures of [Zn(II) and Ni(II)] using [D-Penicilamine & L-Cysteine] in (6). These complex have medicinal, biological, and metabolic enzymatic effects (7). The study of bio-organometallic literature review chemistry has recently attracted a lot of attention (7), which is a combined topic between organometallic and biochemistry. The first example of a bioconjugate of a ferrocene amino acid was created in 1957 using alanine. The classic chalcone scaffold has two possible metal coordination sites, both of which have been proposed to be involved in metal binding in the complexes. Considered the least stable metal interaction, monodentate oxygen coordination I was only proposed for the opposing axial positions in specific octahedral metal complexes (8). Breast cancer (BC) can show itself suddenly or manifest as recurring illness after primary (local) therapy is finished. Current care for this disease is palliative once a physical examination, radiological testing, and pathology have confirmed the diagnosis (9). Over 1 million women globally and 41,000 women in the United States lose their lives to BC each year, despite the fact that targeted and systemic medicines are becoming more widely available. There is an urgent need for new techniques for prognostic stratification, particularly with regard to endocrine medications, in order to more accurately estimate the survival benefit from innovative potential treatments in prospective, randomized clinical studies (9). Enzyme inhibitors are substances that temporarily or permanently interact with enzymes in some way, reducing the pace of an enzyme-catalyzed process or preventing enzymes from functioning normally (10).

Experimental part

Physical techniques such FT-IR, UV-Vis, emission, 1H-NMR, 13C-NMR, and melting points were mostly used to characterize the ligand and their complexes. The molar conductivity was assessed using the HANNA HI2300 microprocessor conductivity meter model using DMSO as the solvent. The complex's magnetic susceptibility was calculated using the Faraday technique.

General Procedure for the Preparation of Chalcone (HL1), (E)-1-(2-hydroxyphenyl)-3-(4-methoxyphenyl)prop-2-en-1-one and their complexes

The experiment for the prepared of chalcone (HL1) was started by adding (0.68 gm, 5 mmol) of 2-hydroxyacetophenone into 5ml of ethanol in a round bottom flask, then (0.68 gm, 5 mmol) of 4-methoxybenzaldehyde was added to the flask. The sodium hydroxide solution (0.4 gm, 10 mmol) was then added to the mixture, the addition was done by dripping slowly while stirring with a stirrer (11). The mixture was

mixed with a stirrer 24 hours at room temperature. Cold hydrogen chloride was added to the mixture at a ratio of 10% Set's the pH of the reaction medium to neutral. The resulting crude product is then filtered using a Buchner filter and neutralized by washing with cold ethanol and cold distilled water. Furthermore, recrystallization with ethanol is carried out using a Buchner filter until the precipitate is separated from the filtrate (12). The filtrate is next dried and evaporated at room temperature. As shown in fig.1.

The general procedure for prepared of the Complexes was started, chalcone (HL1) (0.508 g, 2 mmole) dissolved in 5 mL of ethanol, serine (HL4) (0.178 g, 2 mmole) dissolved in 5 mL of mixed solvent (ethanol and water) and were added to a 5 ml of metal chloride (2 mmole) (where M = Co(II), Ni(II), Cu(II), Zn(II), and Cd(II) ; L1 and HL4 = ligands) in ethanol, which was being stirred. The mixture that resulted was stirred for 3 hour. Using 5% potassium hydroxide, the solution's PH was brought down to (7-8). The mixture was then filtered, washed with more ethanol and distilled water, and allowed to dry at room temperature (24 hours) (13). As shown in Fig. 1.

Figure 1: General of synthesis route of the ligand (HL1) and their complexes.

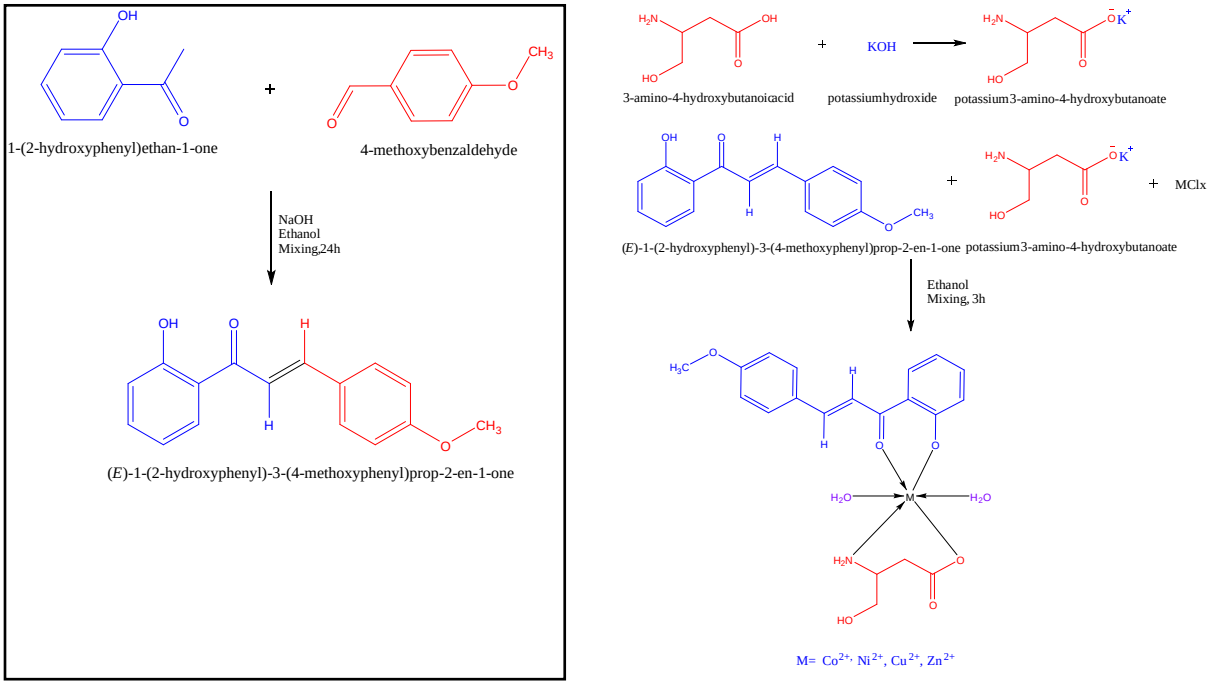

Anticancer activity

Cell culture

MCF-7 cells were maintained in RPMI-1640 supplemented with 10% Fetal bovine serum, 100 units/mL penicillin, and 100 µg/mL streptomycin. Cells were passaged using Trypsin-EDTA reseeded at 80% confluence twice a week, and incubated at 37° (14, 15).

Cytotoxicity assays

96-well plates were used for the MTT test to determine the cytotoxic potential of ligand (HL1) and their copper complex (16, 17). The cell lines were seeded with 1×104 cells per

well. The ligand (HL1) ligand and their copper complex were administered to the cells 24 hours later or when a confluent monolayer was attained. After removing the medium, 28 µL of a 2 mg/mL MTT solution was added, and incubating the cells for 2.5 h at 37 °C after 48 hours of treatment. The residual crystals in the wells were solubilized after the MTT solution was removed by adding 130 µL of DMSO (Dimethyl Sulphoxide), which was then incubated for 15 minutes at 37 °C while being shaken (18). A microplate reader at 492 nm was used to measure the absorbency, and the test was carried out three times. The following equation was used to compute the percentage of cytotoxicity, or the inhibition rate of cell growth(19, 20):-

(Inhibition rate = A- B/A*100)

where A is the control's optical density and B is the samples optical density (21).

To observe the morphology of the cells using an inverted microscope, the cells were seeded into 24-well micro-titration plates at a density of 1 × 105 cells mL-1 and incubated for 24 h at 37 °C. Following that, ligand (HL1) and their copper complex were presented to cells for 24 hours. After the exposure time , the plates were stained with crystal violet stain and incubated at 37 °C for 10–15 min (22). The stain was washed off gently with tap water until the dye was completely removed. The cells were observed under an inverted microscope at 100× magnification and the images were captured with a digital camera attached to the microscope (22). GraphPad Prism 6 was used to statistically evaluate the acquired data using an unpaired t-test (23). The data were displayed as the mean standard deviation of three measurements (23).

In vitro xanthine oxidase inhibitor assay

Assay for the inhibitory action of Xanthine Oxidase (XO) By measuring the amount of uric acid produced during the process catalyzed by xanthine oxidase using UV Spectrophotometry, the activity of xanthine oxidase inhibition may be determined (24).

The working technique was adapted from Sri Wahyuningsih's procedure (25). This study began with the collection of a 10 ml blood sample from a gout patient. The sample was then put in a gel tube, and the serum was separated using a centrifuge. 100 l of the test material was added together with 1.9 ml of 50 mM phosphate buffer pH 7.4 and 1 ml of 0.15 mM xanthine, and the mixture was then incubated at 37°C for 10 minutes. After incubation, 100 l of serum was added, and the mixture was then incubated at 37 °C for 30 minutes. At 290 nm, absorbance was then measured. Measure the percentage of inhibition by comparing the absorbance of the mixture containing test complex to the absorbance of the mixture without test complex (blank samples) (26). Without adding the enzymes, controls were carried out in the same way as the sample group. Calculating xanthine oxidase inhibition

% xanthine oxidase inhibition = (1-B / A) x 100%

Description

A: absorbance without sample (absorbance with enzyme – absorbance without enzyme).

B: absorbance changes by the sample test solution (absorbance Samples with enzyme – absorbance sample without enzyme).

The ligand (HL1) and their complexes with cobalt and copper were used in the test at a variety of concentrations at (1.5, 2, 2.5, 3)*10-

5 Molary. The aim of the Xanthine oxidase inhibition test on ligand and complexes and the findings of fractionation is to analyze how the concentration of the test material affects the rise in inhibition. The substrate has a concentration of 1.5*10-5 Molarty. By analyzing the linear regression of a series of various sample concentrations against percent inhibition, the IC50 values were determined.

Antibacterial activity

The antibacterial activity of ligand (HL1) and their complexes was evaluated using disc diffusion experiments using the Kirby-Bauer technique. Staphylococcus aureus, Escherichia coli, and Burkholderia cepacia clinical bacterial isolates were collected from Anbar University, Department of Biology, College of Science, where their sensitivity to standard antibiotics was also studied. Muller-Hinton agar and the agar well diffusion method were used to measure the clear zone of inhibition. Different solutions of ligand (HL1) and complexes were prepared at (10-2, 10-3, 10-4) molar , incubated at 37 °C for 24 hours, and the results were recorded by measuring the diameter of inhibition in millimeters with a ruler (27).

Result and Discussion

The metal complexes were stable at room temperature, solid, colored, and hygroscopic. The ligand and the complexes' physical and analytical details are shown in Table 1.

Table 1: The Some Physical Properties of the Mixed [L1 - Metal – L4 -2H2O] Complexes

Complex	Empirical Formula	M. wt Calc.	Color	M .P °C	Yield %	$\Lambda m\ \Omega^{-1}\ cm^2\ mol^{-1}$	μeff.(B.M.)
$[Co(L^1)(L^4)(H_2O)_2]$	$C_{19}H_{23}CoNO_8$	452.33	Green-brown	169-172	80	3.5	5.07
$[Ni(L^1)(L^4)(H_2O)_2]$	$C_{19}H_{23}NNiO_8$	452.09	Brown	145-147	62	3.4	2.89
$[Cu(L^1)(L^4)(H_2O)_2]$	$C_{19}H_{23}CuNO_8$	456.94	Yellow-brown	151-154	79	0.3	1.89
$[Zn(L^1)(L^4)(H_2O)_2]$	$C_{19}H_{23}NO_8Zn$	458.77	Pale yellow	138-140	67	0.7	Diamagnetic
$[Cd(L^1)(L^4)(H_2O)_2]$	$C_{19}H_{23}CdNO_8$	505.8	Pale yellow	147-150	73	1	Diamagnetic

FT-IR Spectra

The FT-IR spectra for the ligand (HL1) allocated as shown in (Fig. 2) is as follows: at 2885 cm-1 the appearance of a broad band ascribe to (O-H stretching vibration) (28), this peak appeared in the low frequency region because intermolecular hydrogen band resonates at the lower field (29, 30(.The carbonyl group (C=O stretching vibration) is the source of the band at 1639 cm-1 (31). The peaks appeared at (1539, 1512, 1442 and 1303) cm-1 assigned to aromatic carbons (C=C stretching vibrations) (32). The peaks appeared at 1357cm-1 ascribed to (the methyl groups in acetophenone) and at 1029 cm-1 ascribed to alkyl aryl ether (OCH3 stretching vibrations) (33).

The FT-IR spectra of the serine (HL4) as shown in (fig. 3). The peak appeared at 3471 cm-1 refer to (O-H stretching vibrations) (34). The band appeared at 3082cm-1 assigned to (N-H stretching vibration) (34). The absorption band at 1620 cm-1 was attributed to the (C=O stretching vibration) for carboxyl group (34).

The metal complexes distinctive bands (FT-IR) spectra are assigned in Figures (4 to 8) and are compared to free ligands. The FT-IR spectrum In ligand serine (HL4), the peak that belongs to the hydroxyl group, which appears within 3471 cm-1 as showing in (fig. 3), This peak appears to be downshifting in all complexes about (3444-3414) cm-1 (35), and their peak is attributed to aqueous in all complexes. In the ligand HL1 spectrum The lack of hydroxyl group (OH) at 2835 cm-1 shows that the phenolic group was deprotonated and that the phenolic oxygen was coordinated to the metal ion (36). The N-H stretching vibration of the main amine is attributed to the sharp band that the free ligand (HL4) shows at 3082 cm-1. After complexation, all of the complexes showed this band at a higher frequency, about (3286-3267) cm-1 (35).In The free ligand(HL1) a strong band is observed around 1639 cm−1 due to (C=O stretching vibration), This band has been shifted to a lower or higher frequency appeared about (1620-1639) cm-1 in all the complexes (37). A strong frequency band about (1562-1593) cm−1 assigned to the (COO- stretching vibration) in all the complexes. At 1029 cm-1 ascribed to alkyl aryl ether (OCH3 stretching vibrations) in (HL1), This peak shifted to a lower or higher frequency at about (1014-1041) cm-1 in all complexes (38). In the ranges (528-586) cm-1 and (432-486) cm-1, new weak intensity bands were seen that can be attributed to (M-N) and (M-O), respectively, vibrations (35, 37).

Figure 2: FT-IR spectrum of chalcone (HL1)

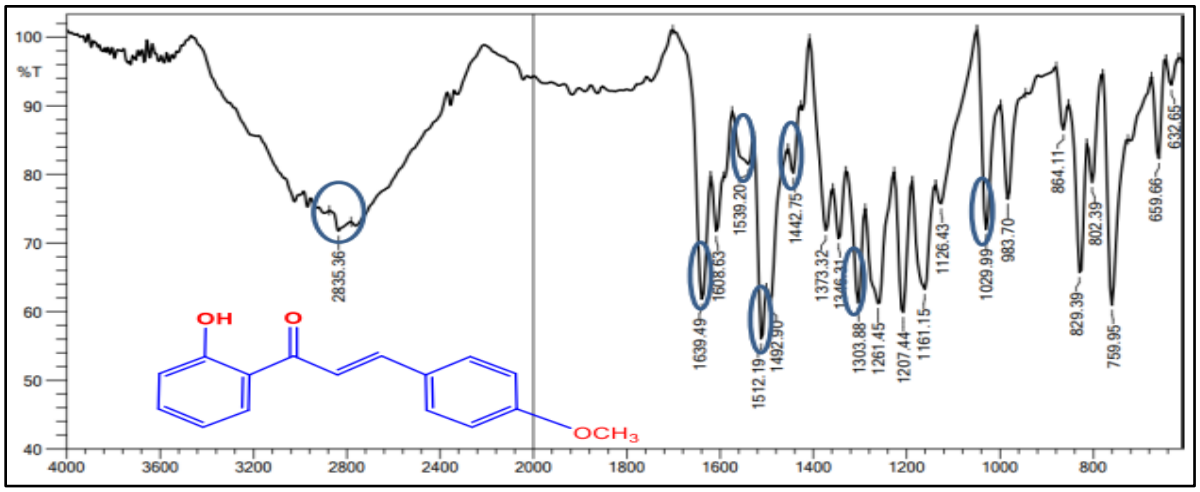

Figure 3: FT-IR spectrum of ligand (HL4).

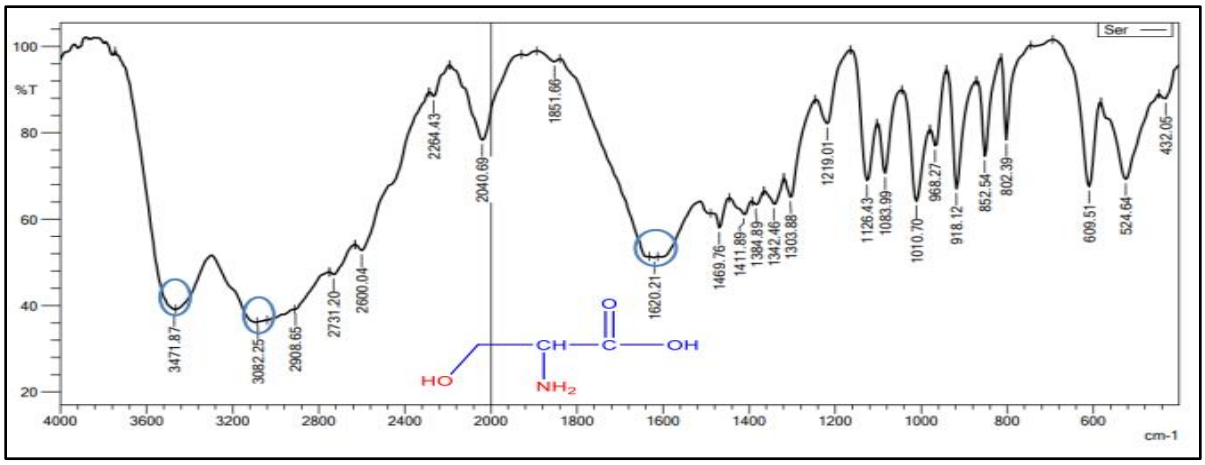

Figure 4: FT-IR spectrum of [Co(L1)(L4)(H2O)2] complex

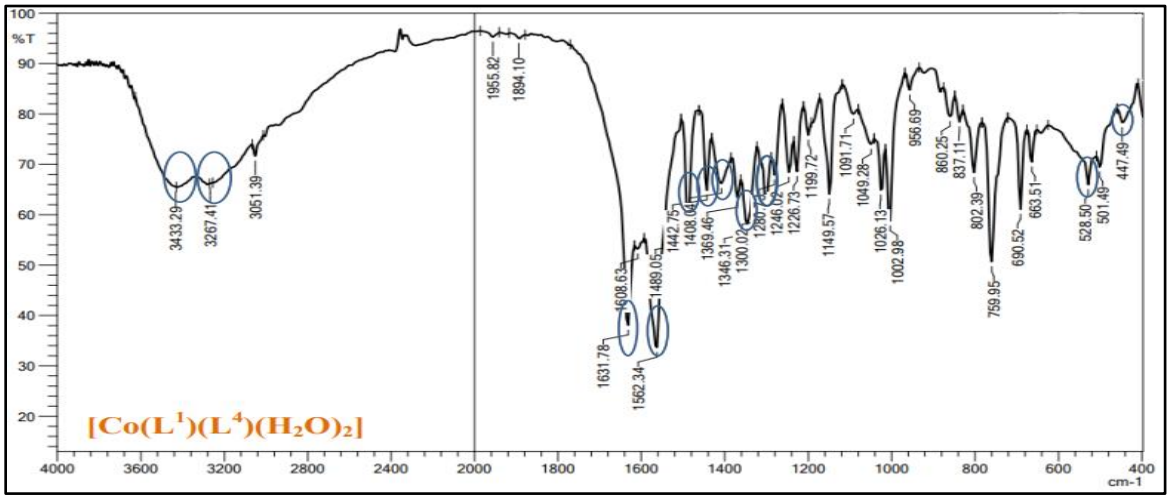

Figure 5: FT-IR spectrum of [Ni(L1)(L4)(H2O)2] complex.

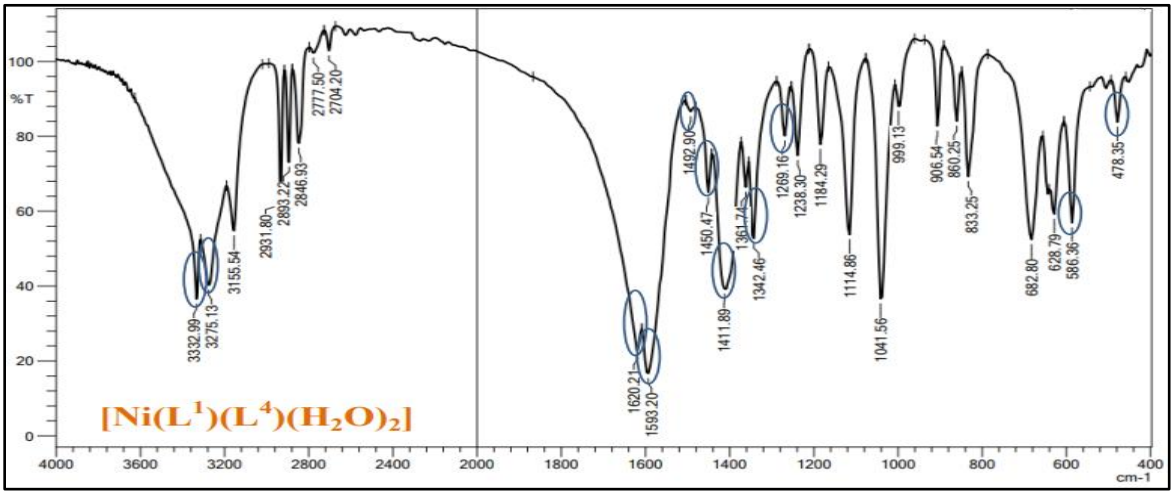

Figure 6: FT-IR spectrum of [Cu(L1)(L4)(H2O)2] complex

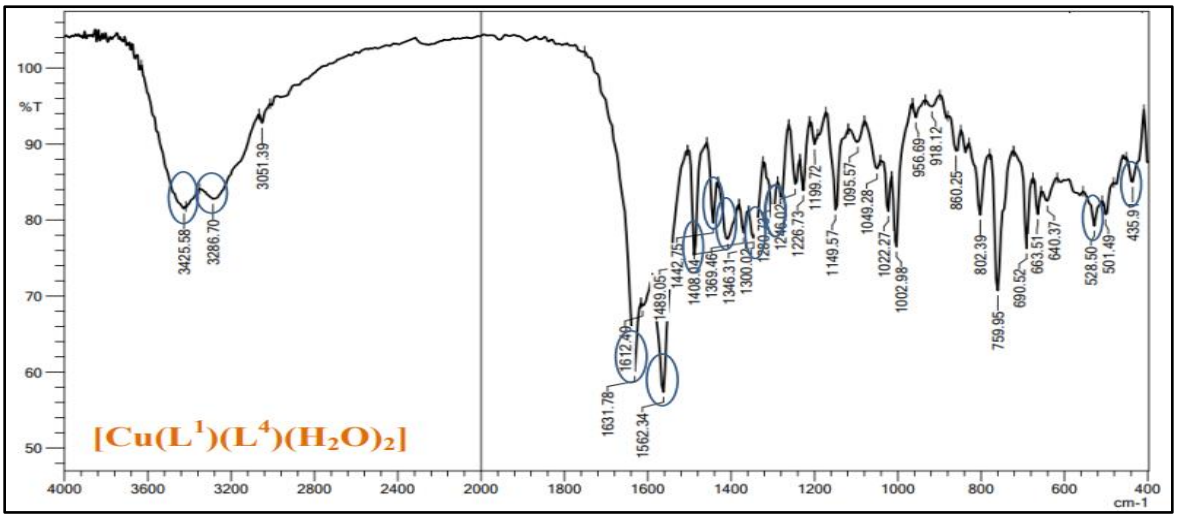

Figure 7: FT-IR spectrum of [Zn(L1)(L4)(H2O)2] complex

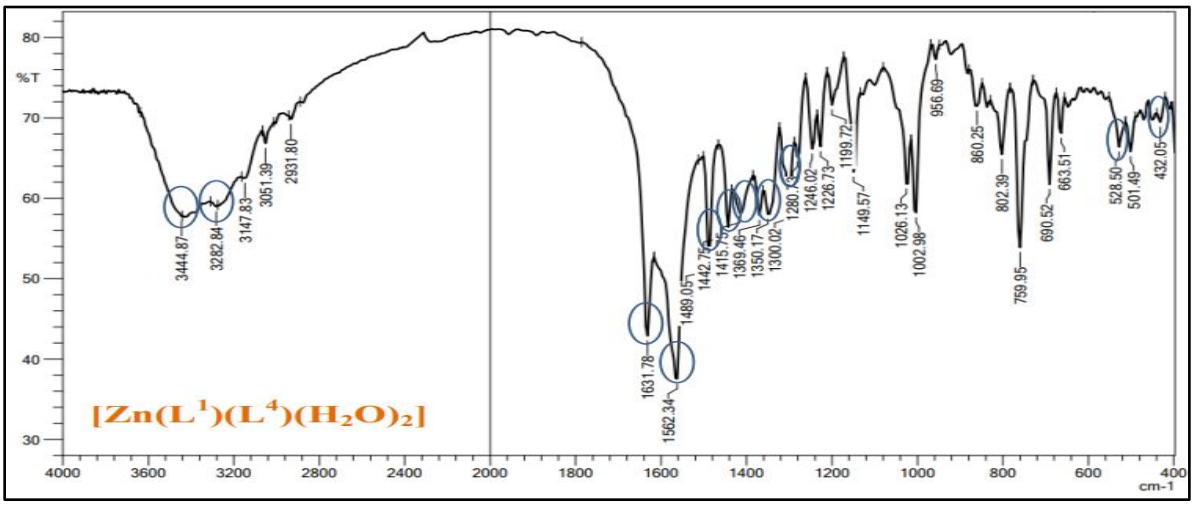

Figure 8: FT-IR spectrum of [Cd(L1)(L4)(H2O)2] complex

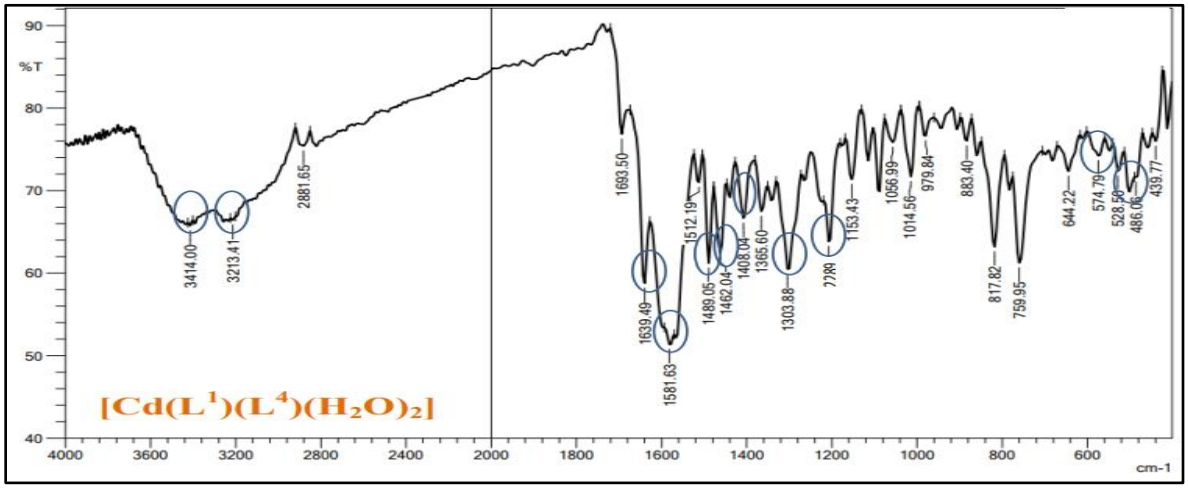

Ultraviolet-Visible Spectrum

Three absorption peaks may appear in the UV-Vis spectra of HL1 in DMSO Fig. 9 (A). peak appeared at (256 nm, 39062 cm-1) and was described as a ligand field transition type π → π * transition. Peaks at (355 nm, 28169 cm-1) and (368 nm, 27173 cm-1) were attributable to the n → π * transition (39).

The Fig. 9 (B), which depicts the UV-Vis spectra of the ligand (HL4) in DMSO, identifies one absorption peaks at (208 nm, 48076 cm-1) as the ligand field π → π * transition (40).

The UV-Vis spectra of the Co-complex in DMSO solution displays six peaks, as shown in Fig.9 (C). The firstly four high intense peaks at (258 nm, 38756 cm-1), (326 nm, 30674 cm-1) and (352 nm, 28409 cm-1) and (369 nm, 27100 cm-1) were assigned to the ligand field (L.F). And another peak in the (383 nm, 26109 cm-1) due to charge transfer transition . The peaks are at (444 nm, 22522 cm-1) and (643 nm, 15552 cm-1) assigned to d-d electronic transition types υ 3 = 4T1g(F)→4T1g(P)) and υ 2 = 4T1g(F) → 4A2g(F) transition respectively, confirming an octahedral structure around Co (II) central metal ion (41).

The electronic spectrum of Ni-complex fig. 9 (D) showed three high intense peaks in the (260 nm, 38461 cm-1), (354 nm, 28248 cm-1) and (365 nm, 27397 cm-1) were assigned to the ligand field (L.F). Another peak in the (379 nm, 26385 cm-1) due to charge transfer transition. The peaks in visible region at (475 nm, 21052 cm-1) and (500 nm, 200000 cm-1). This peaks are assigned to the d-d electronic transition type υ 3 = 3A2g(F)→ 3T1g(P) and υ 2 = 3A2g(F) → 3T1g(F) transition confirming an octahedral structure around Ni (II) ion complex (42).

The electronic spectrum of Cu-complex Fig. 9 (E) showed two intense peaks in the range (257 nm, 38910 cm-1), (355 nm, 28169 cm-1) and (366 nm, 27322 cm-1) are assigned to the ligand field. Another peak in the (445 nm, 22471 cm-1) due to charge transfer transition . The peak is at (497 nm, 20120 cm-1) is assigned to the d-d electronic transition type (2Eg →2T2g) transition confirming a distorted octahedral structure around Cu (II) ion complex (43).

The electronic spectrum of Zn-complex fig. 9 (F) showed four high intense peaks in the (261 nm, 38314 cm-1), (328 nm, 30487 cm-1), (357 nm, 28011 cm-1) and (378 nm, 26455 cm-1) were assigned to the ligand field (L.F). And another peak in the (391nm=25575cm-1) due to charge transfer transition . confirming an octahedral structure around Zn (II) ion complex (44).

The electronic spectrum of Cd-complex fig. 9 (G) showed three high intense peaks in the (258 nm, 38759 cm-1), (356 nm, 28089 cm-1), and (375 nm, 26666 cm-1) were assigned to the ligand field (L.F). And another peak in the (390 nm, 25641 cm-1) due to charge transfer transition confirming an octahedral structure around Cd (II) ion complex (44).

Figure 9: UV-vis spectrum of(A-HL1), (B- L4), (C- Co-complex), (D- Ni-complex), (E- Cu-complex), (F- Zn-complex) and (G- Cd-complex) in DMSO at 10-5M

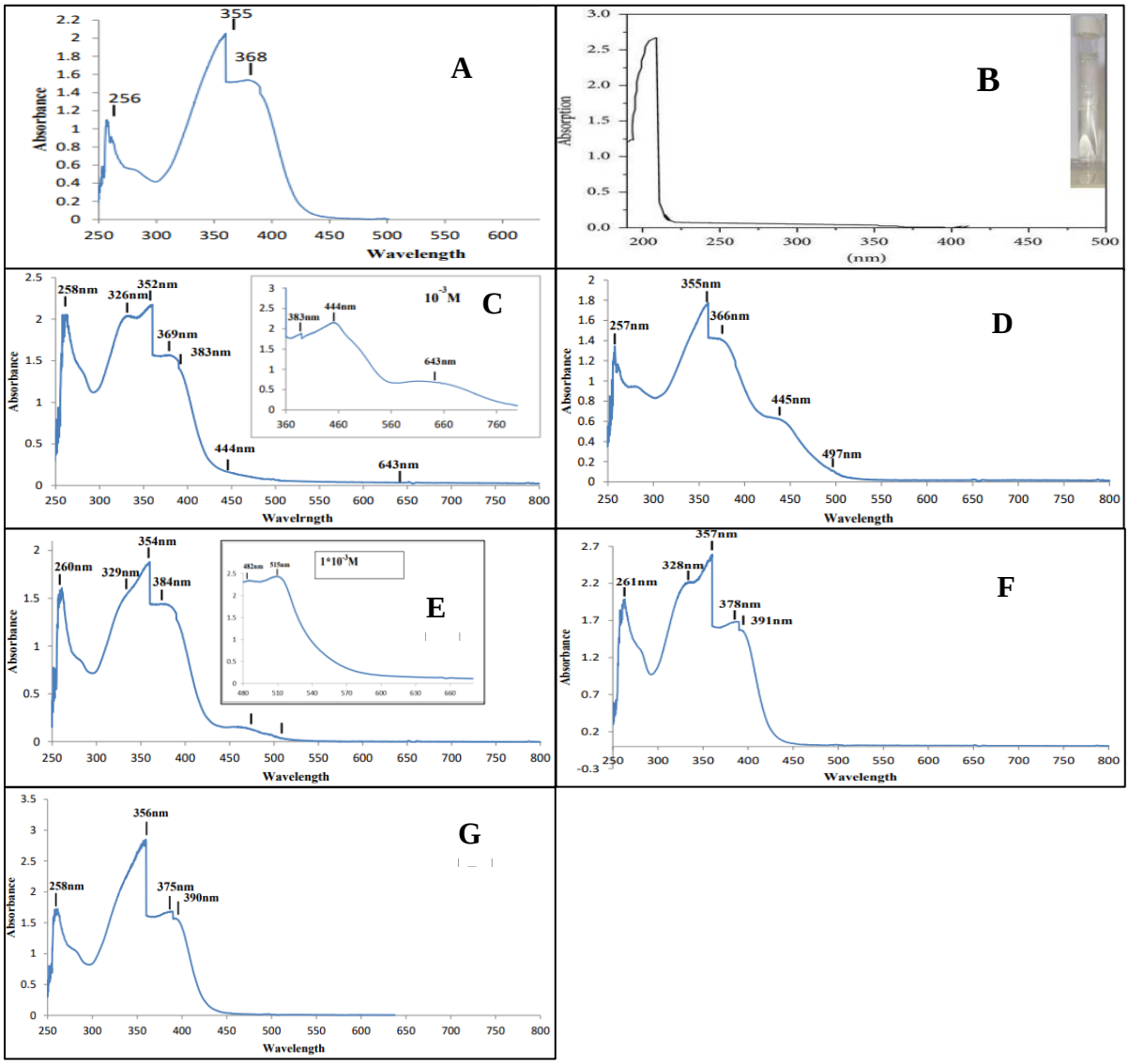

^{1}H-NMR spectrum

The quantity of various types of protons present was found to correlate with the integral intensities of each signal in the ligand (HL1) (Fig. 10) 1H- NMR spectrum. It has been determined that every carbon atom's protons are located in their expected areas (45, 46).

The amplified signals of the (aromatic and,-unsaturated) protons were assigned to the range (6.98- 8.3) ppm in the 1H-NMR (DMSO d6), spectrum of the ligand (HL1). The peak appeared as singlet signal at δ= 3.84ppm, this peak refer to equivalent to three protons of methoxy groups (O-CH3) (47). One group of four resonance signals appointed in range δ (6.98-7.04) ppm ascribed to (C1,12,14-H) proton. The peak as triplet resonance signals at range δ (7.54 -7.58) ppm assigned to (C2,3-H) proton. The peak appeared as multiplet resonance signals at δ (7.82-7.95) ppm (3H) is assigned to (C8,11,15-H) proton (47). The double resonance signals a chemical shift at δ

(8.27 and 8.29)ppm referred to (C4,9-H)proton (47). The chemical shift was detected as a singlet at 12.77 ppm and was attributed to the hydroxyl proton (OH), which resonates with the intermolecular hydrogen band at the lower field (46, 47). At (2.51 and 3.38) ppm, respectively, the 1H-NMR dimethyl sulfoxide solvent and the water residual signals were seen (48).

The recorded 1H-NMR spectrum for [Zn(L1)(L4)(H2O)2] is explained in (Fig. 11). This spectrum displays a triplet chemical shift at δ (2.76-2.81) ppm (1H, t) assigned to (C21-H) proton (49). The complex indicated a quartet resonance signal at δ = 3.25-3.37 ppm (2H, q) assigned to (C19-H) protons (49). The peak appeared as singlet signal at δ = 3.74 ppm (3H, s) attributed to protons of methoxy groups (C28-H, O-CH3) (47), this signal shifted down field compared with the simulation of the free ligand(L1). The doublet chemical shift at δ (5.58 and 5.61) ppm (1H, d) ascribed to (C8-H) proton. The peaks appointed in range δ (6.98-8.29) ppm refer to (O-H, N-H and C1,2,5,6,9,11,12,14,15) protons. The proton of the hydroxyl group (OH) first appeared in the spectrum of the free ligand HL1 with a value of δ= 12.77 ppm; however, the disappearance of this peak indicates that the phenolic group was later deprotonated and its oxygen was coordinated to the metal ion (50). At (2.51 and 3.37) ppm, respectively, the 1H-NMR dimethyl sulfoxide solvent and the water residual signals were seen (48).

Figure 10: 1H-NMR spectrum of ligand HL1 in DMSO-d6

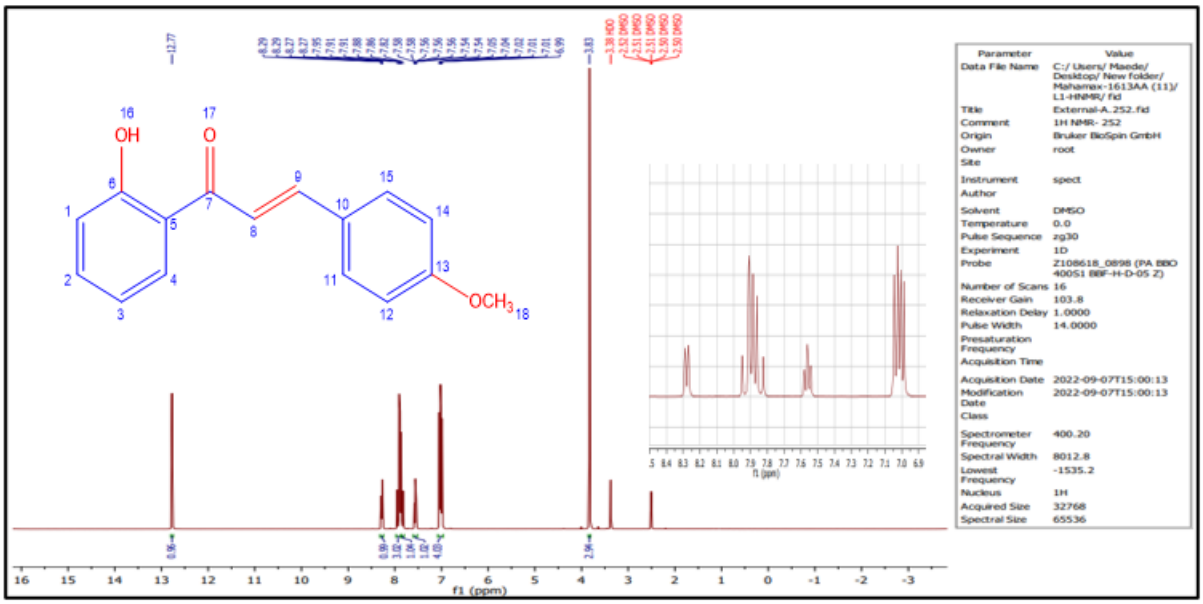

Figure 11: 1H-NMR spectrum of [Zn(L1)(L4)(H2O)2] in DMSO-d6

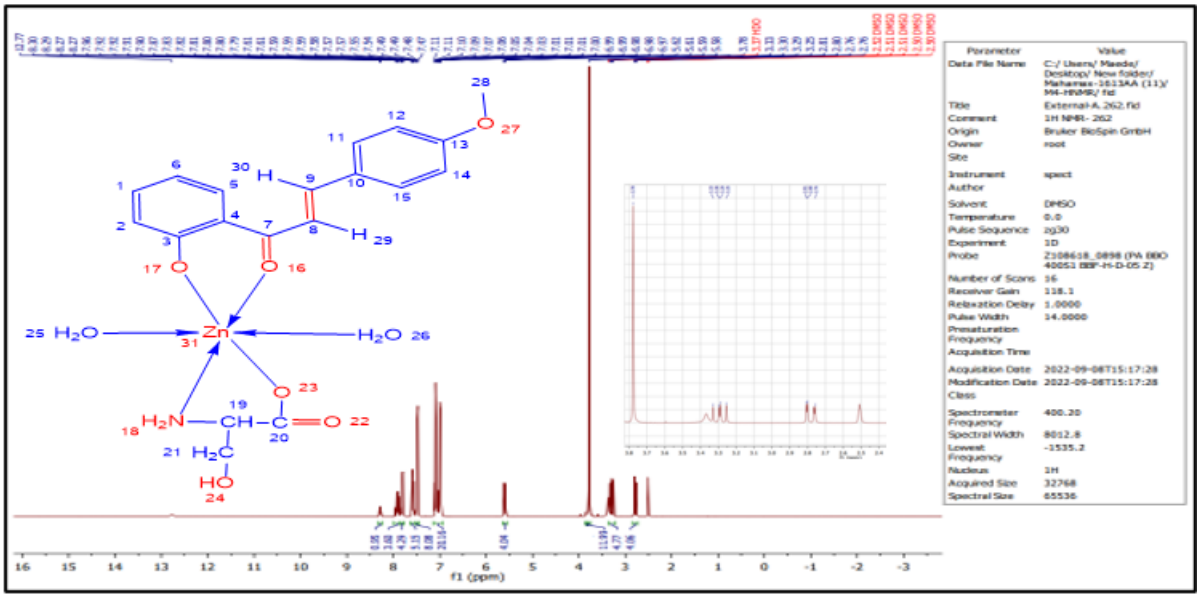

^{13}C-NMR spectrum

It has been determined that every carbon atom in the structure is in its expected area (51). The 13C-NMR spectrum of the ligand (HL1) in DMSO-d6 solvent shown in (Fig. 12).

The formation of the free ligand has been revealed by detecting signal at δ= 55.88ppm which can be attributed to carbon atom C19 for (methoxy group) (52). The peak appeared at δ = 114.94 ppm appointed to carbon atoms C14 and C16 (53). The peaks were appeared at δ (118.19, 119.24, 119.53 and 121.00) ppm refers to carbon atoms C1, C8, C5 and C3, respectively (54, 55). The signal at δ = 127.55 ppm corresponding to carbon atom C10. The peak were appeared at δ = 131.21 ppm ascribed to carbon atom C4 (55). The chemical shift at δ = 131.72 ppm corresponding to carbon atoms C13 and C17. The signals Showed around δ (136.66 and 145.56) ppm assigned to carbons atoms C2 and C9, respectively. This spectrum displays a chemical shift at δ (162.19, 162.56 and 194.04) ppm equivalent to three carbon atoms assigned to C15, C6 and C7, respectively (54). At δ = 40.18 ppm the 13C-NMR dimethyl sulfoxide solvent residual signals were seen (48).

The 13C-NMR spectrum of the ligand [Zn(L1)(L4)(H2O)2] in DMSO-d6 solvent shown in (Fig. 13). The formation of the complex has been revealed by detecting signal at δ = 43.47 ppm ascribed to carbon atom C19 (56). The peak appeared at δ = 55.62 ppm attributed to carbon atom C28 for methoxy group, this signal is shifted down field compared with the simulation of the free ligand (HL1) (53). The chemical shift at δ = 79.06ppm attributed to carbon atom C21(56). The peak at δ = 114.33 ppm appointed to carbon atoms C12 and C14.

The peaks appeared at δ (114.96, 118.90, 121.08,121.80 and 126.77) ppm refers to carbon atoms C8, C4, C2, C6 and C10, respectively (53, 56). The signal at δ = 128.70 ppm corresponding to carbon atom C11 and C15, this signal shifted down field compared with the simulation of the free ligand (HL1). The signals Showed around δ (131.30, 131.72 and 136.69) ppm assigned to carbons atoms C1, C4 and C9, respectively. The spectrum displays

a chemical shift at δ (159.87, 161.63, 162.98 and 192.27) ppm equivalent to three carbon atoms assigned to C3, C13, C7 and C20, respectively (53, 56). The 13C-NMR spectrum for dimethyl sulfoxide solvent were seen at δ = 40 ppm signal (48).

Figure 12: 13C-NMR spectrum of ligand (HL1) in DMSO-d6.

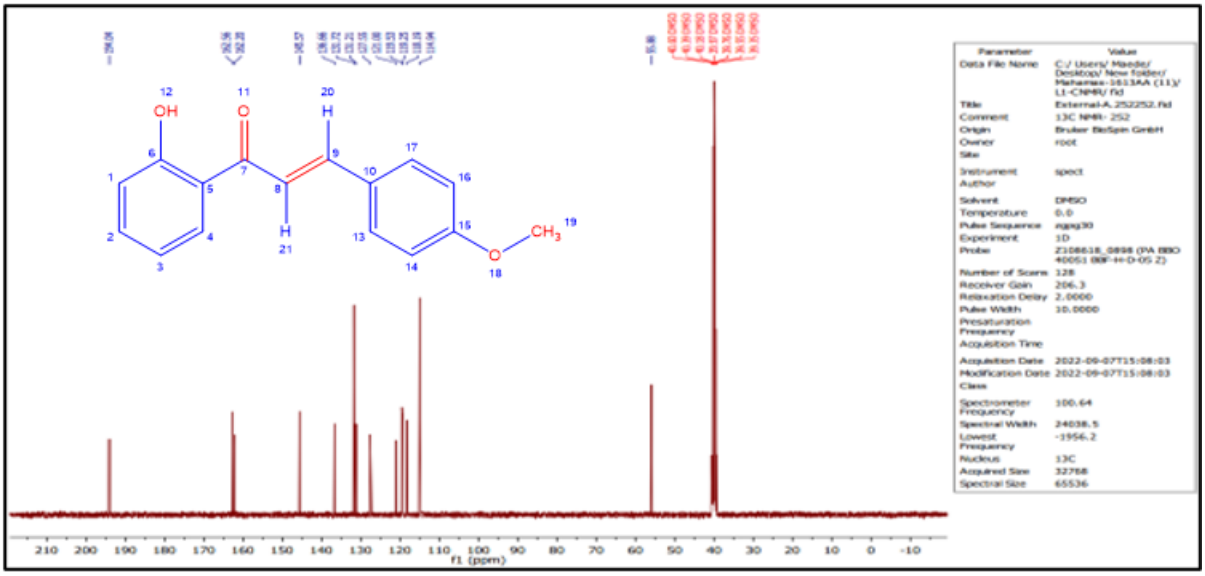

Figure 13: 13C-NMR spectrum of [Zn(L1)(L4)(H2O)2] in DMSO-d6.

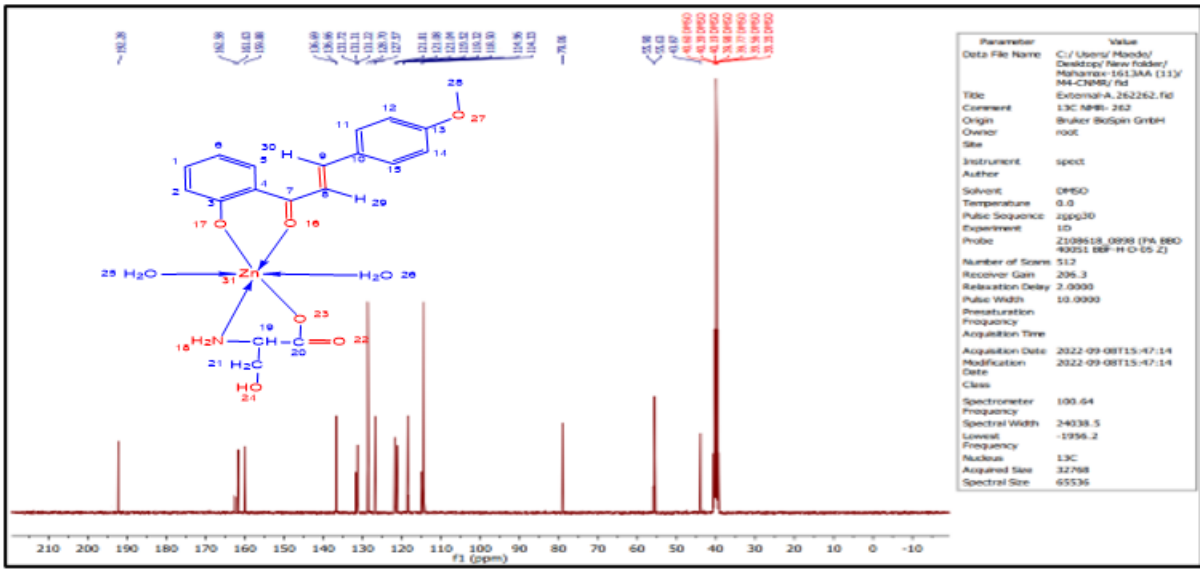

Mass spectrum

The mass spectrum of HL1 is displayed in (Fig. 14). This spectrum reveals subsequent fragments related to the HL1 structure with the appropriate isotope distribution pattern. The parent ion peak for HL1 is observed at m/z= 254.09 (M)•+ for C16H14O3•+; requires =2254.28. The peaks detected at m/z = 237.10, 161.06, 134.07, 108.05 ,81.03 and 51.02 are related to [C16H13O2]+, [C10H9O2]+, [C9H9O]+, [C7H7O]+, [C5H5O]+ and

[C4H3]+ respectively (54, 57). The (fig. 15) illustrates the fragmentation pattern of HL1.

Figure 14: The GC-EI (+) mass spectrum of ligand HL1.

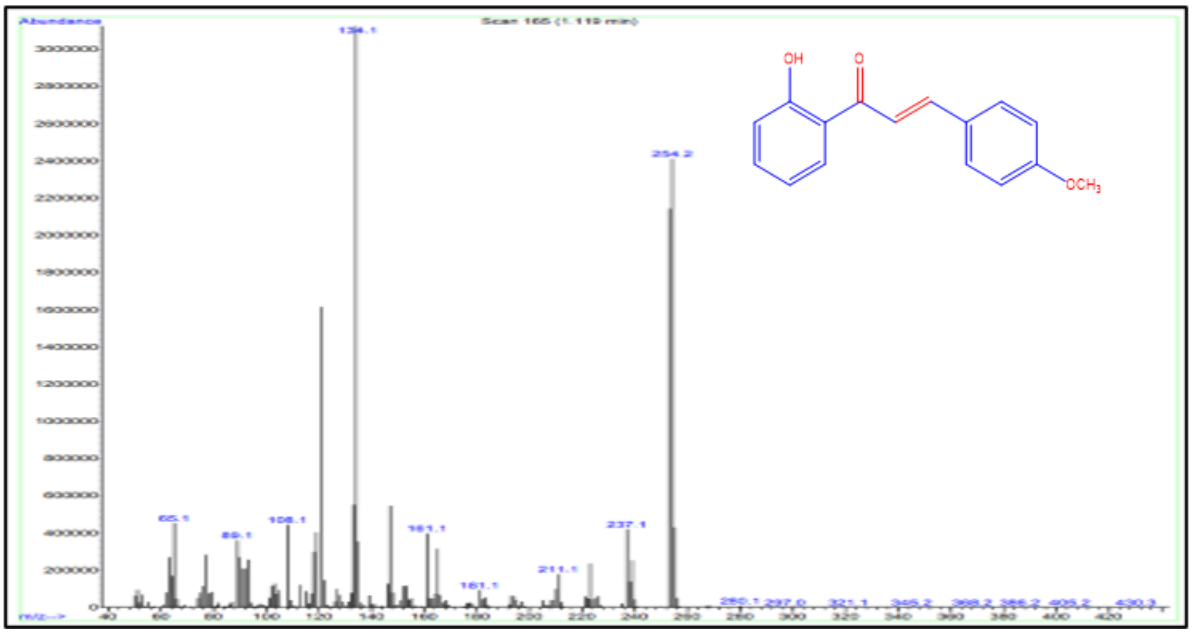

Figure 15: The GC-EI (+) fragmentation pattern of ligand HL1.

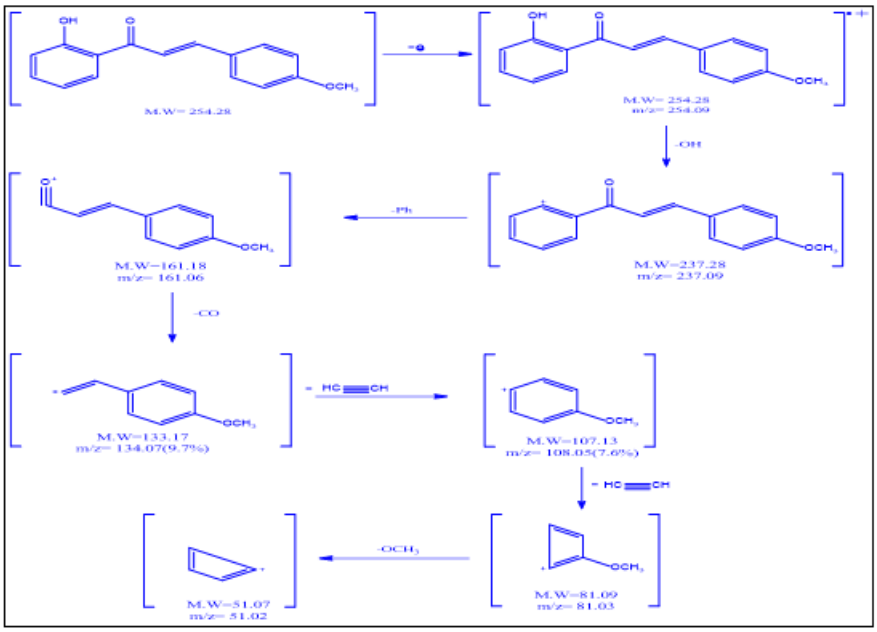

Molar conductivity and magnetic properties for complexes

The measured molar conductivity are (3.5, 3.4, 0.3, 0.7and 1) Ω-1 cm2 mol-1 for [Co(II), Ni(II) ,Cu(II), Zn(II) and Cd(II)] complexes. The results of the silver nitrate (AgNO3) test for the chloride ion were negative, suggesting that the ion is not in the coordination sphere (58). As showed in Table 1.

The magnetic measured was of the prepared Co-complex showed in Table 1, the magnetic value 5.07 B.M., This agreement with octahedral geometry around Co(II) ion (59, 60). Measurements of the prepared Ni-complex showed Table 1 the magnetic value 2.89 B.M., This agreement with octahedral geometry around Ni(II) ion (61). The magnetic value 1.89 B.M. of Cu-complex, this agreement with octahedral geometry around Cu(II) ion (62). The (Zn(II) and Cd(II)) complexes have diamagnetic properties.

Anticancer activity

Recently, the chalcone complexes have gained considerable interest in bioinorganic medicinal chemistry owing to their property with a variety of metals and showing modulatory effect on various anti-cancer targets. In recent past, using chalcone scaffold several potent and less toxic coordinated complexes were developed which showed promising anti-cancer activity(63).

The cytotoxic effect of ligand (HL1) and their copper complexes against MCF-7 cells was studied. The anti-proliferative activity of the ligand (HL1) and their copper complexe was tested by studying their ability to inhibit the cells proliferation. (fig. 16 and fig 17) illustrate the findings, which showed that the investigated compounds had a cytotoxic effect on cancer cell lines MCF-7 (64). The results demonstrated the ability of ligands (HL1) and their copper complexe to make morphological changes in breast cancer cell lines after treated with ligands (HL1) and their copper complexes as in (fig. 18 to fig. 20) (63). The results showed complexes more inhibitor compared with ligands. The results shown cytotoxic effect in AMF-7 cells HL1 = 40.13 µg/ml and IC50 of [Cu(L1)(L4)(H2O)2] = 20.17 µg/ml.

Figure 16: Cytotoxicity of ligand HL1 in MCF-7 cells after 72 hr.

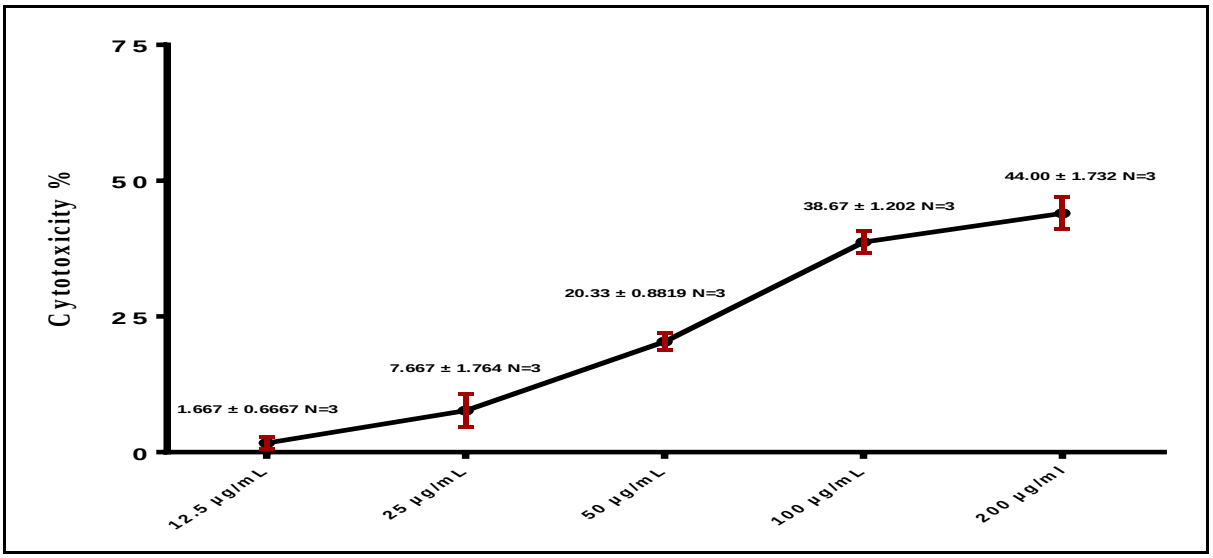

Figure 17: Cytotoxicity of [Cu(L1)(L4)(H2O)2] in MCF-7 cells after 72 hr.

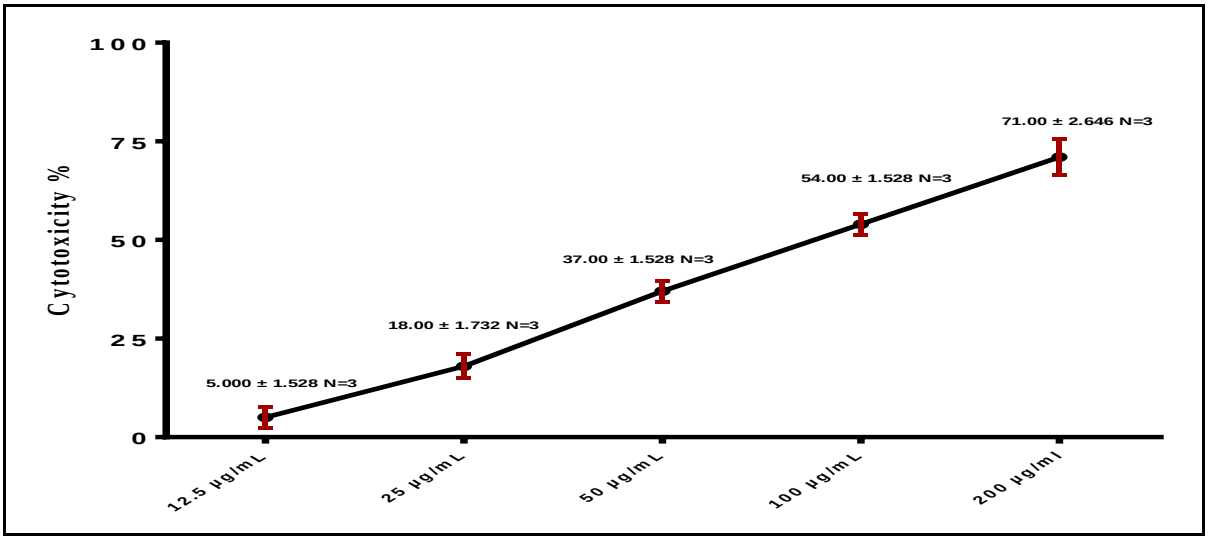

Figure 18: Control untreated MCF-7 cells Magnification power 40x.

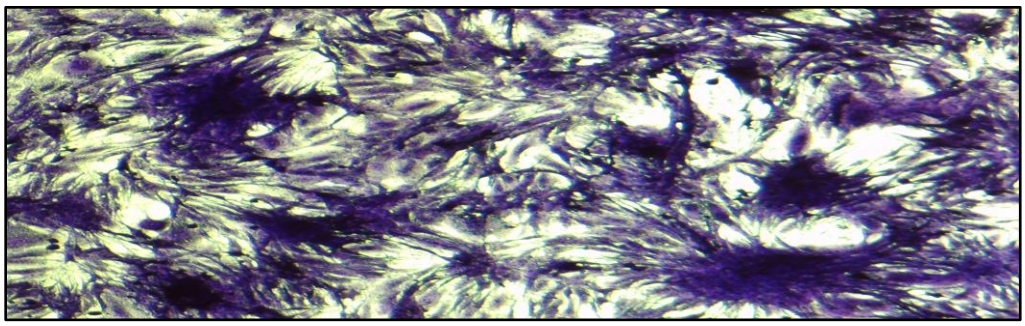

Figure 19: Morphological changes of MCF-7cells after treated with ligand HL1 Magnification power 40x.

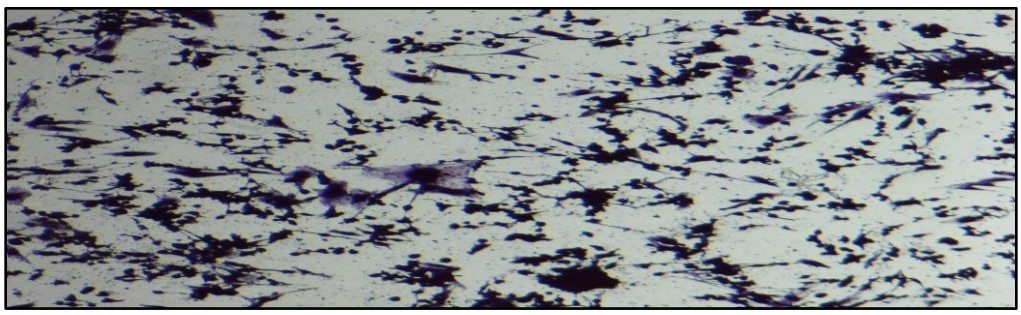

Figure 20: Morphological changes of MCF-7cells after treated with [Cu(L1)(L4)(H2O)2] Magnification power 40x.

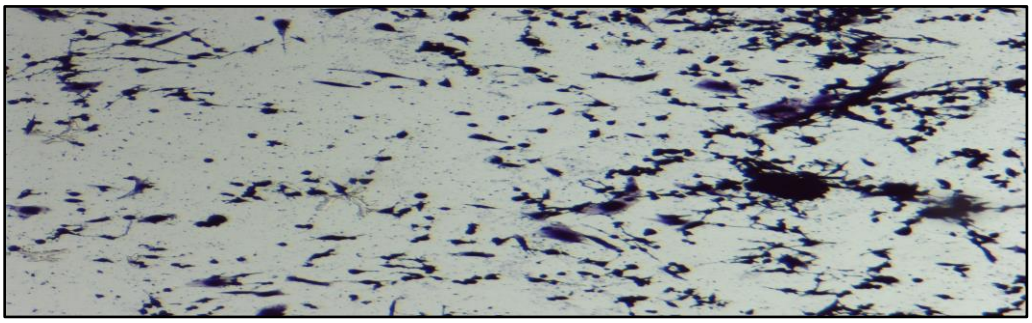

Enzymatic inhibition

As shown in Table 2, results of inhibitory test on xanthine oxidase activity showed that the ligand (HL1) and their complexes with copper and cobalt was tested by studying their ability to inhibiting against xanthine oxidase enzyme (65). The laboratory study showed that ligands and their complexes have an inhibition effect on the xanthine oxidase enzyme (66). The study showed that the complexes of copper and cobalt gave the highest rate of inhibition compared to ligand (HL1). The compounds emerges as an interesting XO inhibitor for the treatment of hyperuricemia and gout with beneficial effects on serum uric acid levels regulating Meanwhile (67). The studies found that the flavonoids or this complexes with a higher affinity for XO, anchor in the active site, more specifically into the hydrophobic pocket of XO, near the molybdenum-pterin domain, in the same channel in which the natural substrate xanthine binds (68). It was also observed that the position of the benzopyranone ring of active flavonoids "sandwiched" between two phenylalanine residues (Phe914 and Phe1009) through aromatic interactions (π–π effects) also contributes to the stability of the complexes, and is important for the flavonoid–XO complexation (68). Metal complexes are increasingly being used to inhibit enzymes. The reasons for this increased interest arise from the special features that metal complexes offer, e.g. the facile construction of 3D architectures that tightly fill enzyme active sites increasing selectivity and the possibility of facile coordination to protein residues that enhances enzyme inhibition (69).

In some cases however, the increased liability of the metal ion allows a more complete exchange of the original ligands with binding residues on potential bio-molecular targets, which in turn reduces selectivity and may account for the general toxicity of the compounds (69). The results shown inhibition of the xanthine oxidase shows through Half-maximal inhibitory concentration (IC50), IC50 of HL1 = 4.79*10-5M, IC50 of [Co(L1)(L4)(H2O)2] = 2.46*10-5M, IC50 of [Cu(L1)(L4)(H2O)2]= 2.7309*10-5M, as shown in table 2.

Table 2: Inhibition rate of xanthine oxidase enzyme by ligands (HL1) and their complexes

Samples	Concentration * 10^{-5}	Inhibition ratio	IC50
HL^1	1.5	5.66	2.81
	2.0	10.06	

	2.5	17.38	
	3.0	25.17	
$[Co(L^1)(L^4)(H_2O)_2]$	1.5	11.26	2.46
	2.0	22.90	
	2.5	39.54	
	3.0	53.10	
$[Cu(L^1)(L^4)(H_2O)_2]$	1.5	13.87	2.30
	2.0	23.26	
	2.5	48.20	
	3.0	60.39	

Antibacterial activities

The (ZI) of the compounds against bacterial growth was supplied in the (table 3) and (fig. 21). The findings showed modest to good activity of the ligand (HL1) and its complexes. Complexes (19, 20, 21, 22, and 23) in a Petri dish are active against Staphylococcus aureus. The complexes (19, 20, 21, 22, and 23) show little anti-Escherichia coli action in a Petri dish. All the complexes showed ineffectiveness against Burkholderia cepacia bacteria. Poor or no action was taken by the (HL1) to combat all types of microorganisms, as shown in table 3.

When used against Staphylococcus aureus, the [Zn(L1)(L4)(H2O)2] and [Cd(L1)(L4)(H2O)2] complexes exhibit excellent antibacterial activity (ZI) more than (20 mm). In general, the produced compound's antibacterial activity occurred in the following sequence; metal complexes > HL1 > DMSO

According to Tweedy's complexes hypothesis (70), the enhanced (ZI) of metal complexes may be explained, indicating that the complexes are more lipophilic than the free ligand HL1.

Table 3 Inhibition zone for the [M(L1)(L4)(H2O)2] complexes

Compounds	Inhibition zone (millimetre)			
	Conc.	*Staphylococcus aureus*	*Escherichia Coli*	*Burkholderia cepacia*
HL^1	10^{-2}	10	8	R
	10^{-3}	9	7	R
	10^{-4}	R	R	R
$[Co(L^1)(L^4)2H_2O]$	10^{-2}	15	11	R
	10^{-3}	11	9	R
	10^{-4}	10	R	R
$[Ni(L^1)(L^4)2H_2O]$	10^{-2}	11	12	R
	10^{-3}	10	9	R
	10^{-4}	8	R	R
$[Cu(L^1)(L^4)2H_2O]$	10^{-2}	1	12	R
	10^{-3}	13	8	R
	10^{-4}	9	R	R
$[Zn(L^1)(L^4)2H_2O]$	10^{-2}	18	11	R
	10^{-3}	13	8	R
	10^{-4}	8	R	R
$[Cd(L^1)(L^6)(H_2O)_2]$	10^{-2}	43	12	R
	10^{-3}	24	R	R
	10^{-4}	11	R	R

Figure 21: Antibacterial activity image, A- [M(L1)(L4)(H2O)2] complexes against Staphylococcus aureus, B- [M(L1)(L4)(H2O)2]complexes against Esherichia Coli, C- [M(L1)(L4)(H2O)2]complexes against Burkholderia cepacia

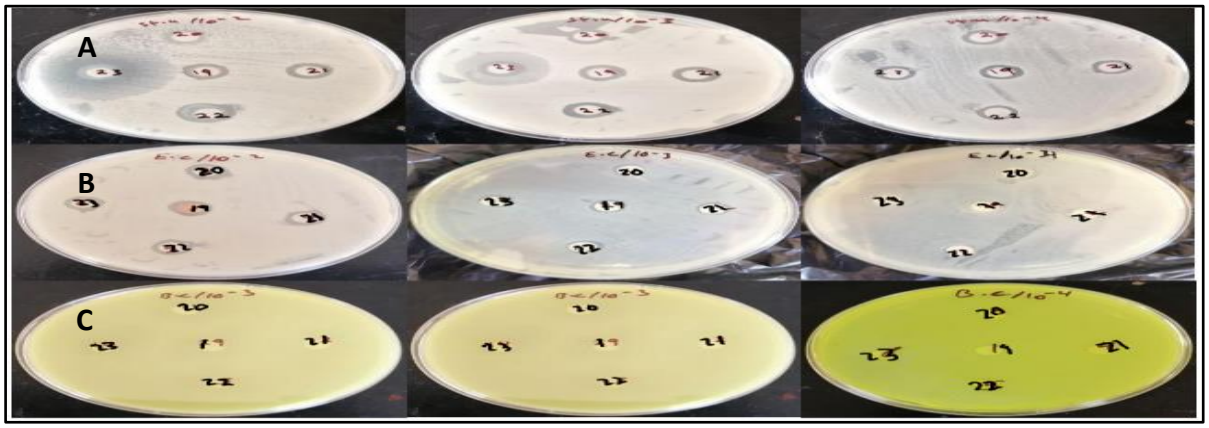

Figure 22: Antibacterial activity image

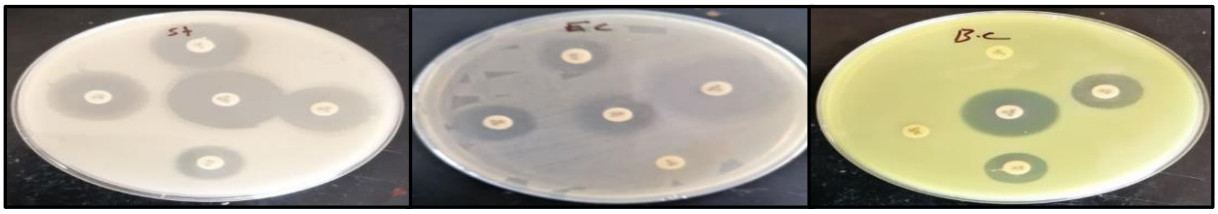

Table 4: Antibiotic activity towards pathogenic bacterial

Antibiotic	Symbol	Inhibition zone (millimetre)		
		Staphylococcus aureus	*Esherichia Coli*	*Burkholderia cepacia*
Oxacillin	OX	28	R	R
Amikacin	AK	18	20	17
Meropenem	MEM	32	40	25
Gentamicin	CN	26	23	18
Shiga toxin	STX	25	25	R

R: Resistant

Conclusions

The ligands (HL1) are successfully synthesized by reaction the 4-methoxybenzaldehyde and 2-hydroxyacetophenone. The prepared ligands (HL1) behaved as bi-dentate. The possibility of preparing complexes from a mixture of ligands (HL1 and HL4), and metal salts (M= Co (II), Ni(II),Cu(II), Zn(II) and Cd(II)) were used. From the UV-Visible study and magnetic moments an octahedral geometry was proposed for mixed HL3 and HL6 complexes. The conductivity experiments revealed that all of the produced complexes are non-conductive, indicating that the complexes contain a neutral charge.FT-IR spectra for synthesized ligands

and complexes revealed vibrational frequencies are comparable to those in theoretical research. The ligands and Zn-complexes in DMSO-d6 revealed signals in their 1H, 13C-NMR spectra that corresponded to various protons and carbon nuclei in accordance with the suggested structural formula. The positive mass spectra for ligands are said to consist of a number of peaks that correspond to consecutive fragmentations of the parent ion molecule, which suggested the production of the precursor ligands and complexes. The anti-proliferative activity of the ligands and their copper complexes was tested by studying their ability to inhibit the cells proliferation. The results demonstrated that the tested materials have cytotoxic effect against cancer cell lines MCF-7.The in vitro study derived from the assays showed that the ligands and their complexes are effective in inhibiting xanthine oxidase enzyme. The synthesised ligands and their complexes exhibit good biological activity against the three bacterial species Staphylococcus aureus(G+), Escherichia coli(G-) and Burkholderia cepacia (G-).

Acknowledgments

The authers would like to acknowledge the contribution of the University of Anbar (www. uoanbar.edu.iq) via their prestigious academic staff in supporting this research with all required technical and academic support, as well as thanks to the Anbar Health Department.

Reference

1. Alam, M. S.; Rahman, S. M.; Lee, D.-U. Synthesis, biological evaluation, quantitative-SAR and docking studies of novel chalcone derivatives as antibacterial and antioxidant agents. Chemical Papers. 2015, 69 (8), 1118– 1129.

2. Singh, P.; Anand, A.; Kumar, V. Recent developments in biological activities of chalcones: A mini review. European journal of medicinal chemistry. 2014, 85, 758– 777.

3. Elkanzi, N. A., Hrichi, H., Alolayan, R. A., Derafa, W., Zahou, F. M., & Bakr, R. B. (2022). Synthesis of chalcones derivatives and their biological activities: a review. ACS omega, 7(32), 27769-27786.

4. Karthikeyan, C.; Narayana Moorthy, N. S.H.; Ramasamy, S.; Vanam, U.; Manivannan, E.; Karunagaran, D.; Trivedi, P. Advances in chalcones with anticancer activities. Recent patents on anti-cancer drug discovery. 2014, 10 (1), 97– 115.

5. McCuistion, L. E., Yeager, J. J., Winton, M. B., & DiMaggio, K. V. (2021). Pharmacology E-Book: A Patient-Centered Nursing Process Approach. Elsevier Health Sciences.

6. Mihai, S., & Negoiu, M. (2009). Synthesis and characterization of Ni (II), Pt (IV), Pd (II), Co (II), Au (III), Cu (II) complexes with mixed ligands. Rev. Chim.(Bucharest), 60, 222.

7. Perrin, D. D., & Agarwal, R. P. (1973). Metal ions in biological systems. Ed. Sigel HC, Vol. 2.

8. Sulpizio, C., Breibeck, J., & Rompel, A. (2018). Recent progress in synthesis and characterization of metal chalcone complexes and their potential as bioactive agents. Coordination Chemistry Reviews, 374, 497-524.

9. Cristofanilli, M., Pierga, J. Y., Reuben, J., Rademaker, A., Davis, A. A., Peeters, D. J., ... & Pantel, K. (2019). The clinical use of circulating tumor cells (CTCs) enumeration for staging of metastatic breast cancer (MBC): International expert consensus paper. Critical reviews in oncology/hematology, 134, 39-45.

10. Kuddus, M. (2019). Introduction to food enzymes. In Enzymes in food biotechnology (pp. 1-18). Academic Press.

11. Septianingtyas, D., Zafira, N., Zulhipri, Kurniadewi, F., & Dianhar, H. (2021, April). Green synthesis of chalcones derivatives. In AIP Conference Proceedings (Vol. 2331, No. 1, p. 040020). AIP Publishing LLC.

12. Al-Obaidi, O. H. (2014). Synthesis, Spectral Characterization, Theoretical Evaluation Of New Co (Ii) And Mn (Ii) Complexes Of Flavone. Journal of Applicable Chemistry, 3(1), 157-163.

13. Mutlu Gençkal, H., Erkisa, M., Alper, P., Sahin, S., Ulukaya, E., & Ari, F. (2020). Mixed ligand complexes of Co (II), Ni (II) and Cu (II) with quercetin and diimine ligands: Synthesis, characterization, anti-cancer and anti-oxidant activity. JBIC Journal of Biological Inorganic Chemistry, 25(1), 161-177.

14. Al-Ziaydi, A. G., Al-Shammari, A. M., Hamzah, M. I., and Jabir, M. S. (2020). Hexokinase inhibition using D-Mannoheptulose enhances oncolytic newcastle disease virus-mediated killing of breast cancer cells. Cancer Cell International, 20(1), 1-10.

15. Al-Ziaydi, A. G., Hamzah, M. I., Al-Shammari, A. M., Kadhim, H. S., and Jabir, M. S. (2020, December). The anti-proliferative activity of D-mannoheptulose against breast cancer cell line through glycolysis inhibition. In AIP Conference Proceedings (Vol. 2307, No. 1, p. 020023). AIP Publishing LLC.

16. Al Salman, H. N. K., Ali, E. T., Jabir, M., Sulaiman, G. M., and Al Jadaan, S. A. (2020). 2 Benzhydrylsulfinyl N hydroxyacetamide Na extracted from fig as a novel cytotoxic and apoptosis inducer in SKOV 3 and AMJ 13 cell lines via P53 and caspase 8 pathway. Eurpean food research and technology.

17. Al-Ziaydi, A. G., Al-Shammari, A. M., Hamzah, M. I., Kadhim, H. S., and Jabir, M. S. (2020). Newcastle disease virus suppress glycolysis pathway and induce breast cancer cells death. VirusDisease, 1-8.

18. Al-Musawi, S., Albukhaty, S., Al-Karagoly, H., Sulaiman, G. M., Jabir, M. S., & Naderi-Manesh, H. (2020). Dextran-coated superparamagnetic nanoparticles modified with folate for targeted drug delivery of camptothecin. Advances in Natural Sciences: Nanoscience and Nanotechnology, 11(4), 045009.

19. Jawad, M., Öztürk, K., and Jabir, M. S. (2021). TNF-α loaded on gold nanoparticles as promising drug delivery system against proliferation of breast cancer cells. Materials Today: Proceedings, 42, 3057-3061.

20. Al-Shammari, A. M., Al-Saadi, H., Al-Shammari, S. M., and Jabir, M. S. (2020). Galangin enhances gold nanoparticles as anti-tumor agents against ovarian cancer cells. In AIP Conference Proceedings (Vol. 2213, No. 1, p. 020206). AIP Publishing LLC.

21. Ibrahim, A. A., Kareem, M. M., Al-Noor, T. H., Al-Muhimeed, T., AlObaid, A. A., Albukhaty, S, and Sahib, U. I. (2021). Pt (II)-Thiocarbohydrazone complex as cytotoxic agent and apoptosis inducer in Caov-3 and HT-29 cells through the P53 and Caspase-8 pathways. Pharmaceuticals, 14(6), 509.

22. Khashan, K. S., Abdulameer, F. A., Jabir, M. S., Hadi, A. A., and Sulaiman, G. M. (2020). Anticancer activity and toxicity of carbon nanoparticles produced by pulsed laser ablation of graphite in water. Advances in Natural Sciences:

Nanoscience and Nanotechnology, 11(3), 035010.

23. Abbas, Z. S., Sulaiman, G. M., Jabir, M. S., Mohammed, S. A., Khan, R. A., Mohammed, H. A., and Al-Subaiyel, A. (2022). Galangin/β-Cyclodextrin Inclusion Complex as a Drug-Delivery System for Improved Solubility and Biocompatibility in Breast Cancer Treatment. Molecules, 27(14), 4521.

24. Hendriani, R., Sukandar, E. Y., Anggadiredja, K., & Sukrasno, S. "In vitro evaluation of xanthine oxidase inhibitory activity of Sonchus arvensis leaves". Int J Pharm Clin Res, vol. 6, pp. 501-3, (2014).

25. Wahyuningsih, S., & ElinYulinahSukandar, S. "In Vitro Xanthine Oxidase Inhibitor Activity of Ethanol Extract and Fraction Roselle Calyx (Hibiscus sabdariffa L.)". Int. J. Pharma. Clin. Res., vol. 94, pp. 5-35, (2016).

26. Widyanto.PS., & Nelistya.A. "Rosella Various processed, efficacy and Potions, Penebar Swadaya, pp. 11-21, (2009).

27. Matuschek, E., Brown, D. F., and Kahlmeter, G. "Development of the EUCAST disk diffusion antimicrobial susceptibility testing method and its implementation in routine microbiology laboratories". Clinical Microbiology and Infection, 20(4), O255-O266, (2014).

28. Leal, A. L., Pinheiro, D. P., Barros-Nepomuceno, F. W., da Silva, P. T., Pessoa, C., Almeida-Neto, F. W., ... & Teixeira, A. M. (2021). Structural and spectroscopic analysis and evaluation of cytotoxic activity of 2-hydroxychalcones against human cancer cell lines. Journal of Molecular Structure, 1245, 131135.

29. Suiter, C. L., Malavé, V. D., Garboczi, E. J., Widegren, J. A., & McLinden, M. O. (2020). Nuclear Magnetic Resonance (NMR) Spectroscopy for the In Situ Measurement of Vapor–Liquid Equilibria. Journal of Chemical & Engineering Data, 65(7), 3318-3333.

30. Lekaa K Abdul Karem, " Synthesis, Characterization And Biological Evaluation of New Schiff Bases Mixed Ligand Metal Complexes of Some Drug Substances", Department of Chemistry, College of Education for Pure Sciences, Ibn/al Haitham, University of Baghdad, (2016).

31. Teixeira, A. M. R., Santos, H. S., Bandeira, P. N., Julião, M. S. S., Freire, P. T. C., Lima, V. N., ... & Sena Jr, D. M. (2019). Structural, spectroscopic and microbiological characterization of the chalcone 2E-1-(2′-hydroxy-3′, 4′, 6′-trimethoxyphenyl)-3-(phenyl)-prop-2-en-1-one derived from the natural product 2-hydroxy-3, 4, 6-trimethoxyacetophenone. Journal of Molecular Structure, 1179, 739-748.

32. Santiago, R. N. S., Freire, P. T. C., Teixeira, A. M. R., Bandeira, P. N., Santos, H. S., Lemos, T. L., & Ferraz, C. A. N. (2018). FT-Raman and FT-IR spectra and DFT calculations of chalcone (2E)-1-(4-aminophenyl)-3-phenyl-prop-2-en-1-one. Vibrational Spectroscopy, 97, 1-7.

33. Custodio, J. M., Vaz, W. F., de Andrade, F. M., Camargo, A. J., Oliveira, G. R., & Napolitano, H. B. (2017). Substitution effect on a hydroxylated chalcone: conformational, topological and theoretical studies. Journal of Molecular Structure, 1136, 69-79.

34. HASAN, H. M. I., & WAHID, S. M. A. (2014). Potentiometric studies on serine and Asparagin complexe with Cd and pb.

35. Jain, U. K., Bhatia, R. K., Rao, A. R., Singh, R., Saxena, A. K., & Sehar, I. (2014).

Design and development of halogenated chalcone derivatives as potential anticancer agents. Tropical Journal of Pharmaceutical Research, 13(1), 73-80.

36. Bentley, R. (2005). Methionine and derivatives: exploring chirality at sulfur. Biochemistry and Molecular Biology Education, 33(4), 274-276.

37. G. R. Fulmer, A. J. M. Miller, N. H. Sherden, H. E. Gottlieb, A. Nudelman, B. M. Stoltz, J. E. Bercaw, K. I. Goldberg," NMR Chemical shifts of trace impurities: common laboratory solvents, organics, and gases in deuterated solvents relevant to the organometallic chemist", Organomet., 29, 9, 2176-2179, (2010).

38. Matuschek, E., Brown, D. F., and Kahlmeter, G. "Development of the EUCAST disk diffusion antimicrobial susceptibility testing method and its implementation in routine microbiology laboratories". Clinical Microbiology and Infection, 20(4), O255-O266, (2014).

39. Serobatse, K. R., & Kabanda, M. M. (2016). A theoretical study on the antioxidant properties of methoxy-substituted chalcone derivatives: A case study of kanakugiol and pedicellin through their Fe (II and III) coordination ability. Journal of Theoretical and Computational Chemistry, 15(06), 1650048.

40. Rajesh, K., & Kumar, P. P. (2014). Structural, linear, and nonlinear optical and mechanical properties of new organic L-Serine crystal. Space, 212121, P212121.

41. KADHIUM, A., MAHDI, S., & AALRAMAHI, F. (2019). Synthesis and Charecterization of New Chalcone-Azo Ligands and Its Transition Metal Mixed Ligands Complexes with A Cytotoxic Activity study of Pd (II) Complex. International Journal of Pharmaceutical Research, 11(4).

42. Sultan, J. S., Lateaf, S. M., & Rashid, D. K. (2015). Synthesis, Characterization and Antibacterial Activity of Mixed Ligand (HL) Complexes Mn (ll), Co (ll), Ni (ll), Zn (ll), Cd (ll) and Hg (ll) with Azide (N 3< sup style=. Open Journal of Inorganic Chemistry, 5(04), 102.

43. Baper, S. H., & Mohammd, M. S. (2022). Synthesis, characterization and study anticancer activity of new Azo–Chalcone with mix Ligand of some divalent metal chelate complexes. JOURNAL OF KUFA FOR CHEMICAL SCIENCES, 2(9).

44. Botha, N. L. (2015). Copper dithiocarbamate complexes and copper sulfide nanoparticles: synthesis, characterization and antifungal studies (Doctoral dissertation, University of Fort Hare).

45. Suiter, C. L., Malavé, V. D., Garboczi, E. J., Widegren, J. A., & McLinden, M. O. (2020). Nuclear Magnetic Resonance (NMR) Spectroscopy for the In Situ Measurement of Vapor–Liquid Equilibria. Journal of Chemical & Engineering Data, 65(7), 3318-3333.

46. Lekaa K Abdul Karem, " Synthesis, Characterization And Biological Evaluation of New Schiff Bases Mixed Ligand Metal Complexes of Some Drug Substances", Department of Chemistry, College of Education for Pure Sciences, Ibn/al Haitham, University of Baghdad, (2016).

47. da Cunha Xavier, J., de Almeida-Neto, F. W., Rocha, J. E., Freitas, T. S., Freitas, P. R., de Araujo, A. C., Teixeira, A. M., "Spectroscopic analysis by NMR, FT-Raman, ATR-FTIR, and UV-Vis, evaluation of antimicrobial activity, and in silico studies of chalcones derived from 2-hydroxyacetophenone", Journal of Molecular Structure, vol.1241, p.p.130647. (2021).

48. G. R. Fulmer, A. J. M. Miller, N. H. Sherden, H. E. Gottlieb, A. Nudelman, B. M. Stoltz, J. E. Bercaw, K. I. Goldberg," NMR Chemical shifts of trace impurities: common laboratory solvents, organics, and gases in deuterated solvents relevant to the organometallic chemist", Organomet., 29, 9, 2176-2179, (2010).

49. Kovalenko, E. A., & Mainichev, D. A. (2015). Supramolecular system of aminoacids and cucurbit [7] uril: NMR studies in solution. Applied Magnetic Resonance, 46(3), 281-293.

50. Borge, V. V., & Patil, R. M. (2020). Stability of Vanadium Chalcone Complexes. Stability and Applications of Coordination Compounds, 59-67.

51. Lekaa K Abdul Karem, " Synthesis, Characterization And Biological Evaluation of New Schiff Bases Mixed Ligand Metal Complexes of Some Drug Substances", Department of Chemistry, College of Education for Pure Sciences, Ibn/al Haitham, University of Baghdad, (2016).

52. Attarde, M., Vora, A., Varghese, A., & Kachwala, Y. (2014). Synthesis and evaluation of chalcone derivatives for its alpha amylase inhibitory activity. Organic Chemistry: An Indian Journal, 10(5), 192-204.

53. da Cunha Xavier, J., de Almeida-Neto, F. W., Rocha, J. E., Freitas, T. S., Freitas, P. R., de Araujo, A. C., Teixeira, A. M., "Spectroscopic analysis by NMR, FT-Raman, ATR-FTIR, and UV-Vis, evaluation of antimicrobial activity, and in silico studies of chalcones derived from 2-hydroxyacetophenone", Journal of Molecular Structure, vol.1241, p.p.130647. (2021).

54. Lima, D. C. D. S., Vale, C. R. D., Véras, J. H., Bernardes, A., Pérez, C. N., & Chen-Chen, L. (2017). Absence of genotoxic effects of the chalcone (E)-1-(2-hydroxyphenyl)-3-(4-methylphenyl)-prop-2-en-1-one) and its potential chemoprevention against DNA damage using in vitro and in vivo assays. Plos one, 12(2), e0171224.

55. Raghav, N., & Garg, S. (2014). SAR studies of o-hydroxychalcones and their cyclized analogs and study them as novel inhibitors of cathepsin B and cathepsin H. European journal of pharmaceutical sciences, 60, 55-63.

56. Aronu, U. E., Ciftja, A. F., Kim, I., & Hartono, A. (2013). Understanding precipitation in amino acid salt systems at process conditions. Energy Procedia, 37, 233-240.

57. Gao, X., Williams, S. J., Woodman, O. L., & Marriott, P. J. (2010). Comprehensive two-dimensional gas chromatography, retention indices and time-of-flight mass spectra of flavonoids and chalcones. Journal of Chromatography A, 1217(52), 8317-8326.

58. Alkhafagi, Z. H., & Al-Noor, T. H. (2020, December). Synthesis, characterization and antimicrobial studies of mixed ligand from phthalic acid and 1, 10-phenanthroline with their complexes. In AIP Conference Proceedings (Vol. 2290, No. 1, p. 030031). AIP Publishing LLC.

59. Hussaini, S. Y., Haque, R. A., & Razali, M. R. (2019). Recent progress in silver (I)-, gold (I)/(III)-and palladium (II)-N-heterocyclic carbene complexes: A review towards biological perspectives. Journal of Organometallic Chemistry, 882, 96-111.

60. Kalanithi, M., Rajarajan, M., Tharmaraj, P., & Sheela, C. D. (2012). Spectral, biological screening of metal chelates of chalcone based Schiff bases of N-(3-aminopropyl) imidazole. Spectrochimica

Acta Part A: Molecular and Biomolecular Spectroscopy, 87, 155-162.

61. Sumathi, S., Tharmaraj, P., Sheela, C. D., & Ebenezer, R. (2011). Synthesis, spectral, bioactivity, and NLO properties of chalcone metal complexes. Journal of Coordination Chemistry, 64(10), 1707-1717.

62. Borge, V. V., & Patil, R. M. (2019). Syntheses and characterization of copper metal complexes prepared from chalcone derivatives. Microchemical Journal, 145, 456-459.

63. Mahapatra, D. K., Bharti, S. K., Asati, V., & Singh, S. K. (2019). Perspectives of medicinally privileged chalcone based metal coordination compounds for biomedical applications. European journal of medicinal chemistry, 174, 142-158.

64. Da Silva, J. G., Despaigne, A. A. R., Louro, S. R., Bandeira, C. C., Souza-Fagundes, E. M., & Beraldo, H. (2013). Cytotoxic activity, albumin and DNA binding of new copper (II) complexes with chalcone-derived thiosemicarbazones. European Journal of Medicinal Chemistry, 65, 415-426.

65. Hofmann, E., Webster, J., Do, T., Kline, R., Snider, L., Hauser, Q., ... & Paula, S. (2016). Hydroxylated chalcones with dual properties: Xanthine oxidase inhibitors and radical scavengers. Bioorganic & medicinal chemistry, 24(4), 578-587.

66. Yang, C., Liu, Y., Tu, Y., Li, L., Du, J., Yu, D., ... & Li, Y. (2023). Chalcone derivatives as xanthine oxidase inhibitors: synthesis, binding mode investigation, biological evaluation, and ADMET prediction. Bioorganic Chemistry, 131, 106320.

67. Scotti, L., Júnior, F. J., Ishiki, H. M., Ribeiro, F. F., Duarte, M. C., Santana, G. S., ... & Scotti, M. T. (2018). Computer-aided drug design studies in food chemistry. In Natural and Artificial Flavoring Agents and Food Dyes (pp. 261-297).

68. Scotti, L., Júnior, F. J., Ishiki, H. M., Ribeiro, F. F., Duarte, M. C., Santana, G. S., ... & Scotti, M. T. (2018). Computer-aided drug design studies in food chemistry. In Natural and Artificial Flavoring Agents and Food Dyes (pp. 261-297).

69. Kilpin, K. J., & Dyson, P. J. (2013). Enzyme inhibition by metal complexes: concepts, strategies and applications. Chemical Science, 4(4), 1410-1419.

70. Tweedy, B. G. (1964, January). Possible mechanism for reduction of elemental sulfur by monilinia fructicola. In Phytopathology (Vol. 54, No. 8, p. 910). 3340 PILOT KNOB ROAD, ST PAUL, MN 55121: Amer Phytopathological Soc.